ADVANCED THERMOELECTRIC PERFORMANCE IN InSb–(Sb, Mg_3Sb_2) EUTECTIC COMPOSITES

M.V. KAZIMOV, G.B. IBRAGIMOV, I.S. RAMAZANOVA, U.V. YUSIFOVA, A.F. NURALIEV, G.Kh. GUSEYNOVA, F.F. YAHYAYEV

The Ministry of Science and Education of the Republic of Azerbaijan, Institute of Physics, G.Javid ave 131, AZ1073 Baku

E-mail: mobilkazimov@gmail.com

The InSb–(Sb, Mg_3Sb_2) eutectic composites synthesized via the Bridgman method were systematically characterized using structural analysis, differential scanning calorimetry (DSC), Raman spectroscopy, and X-ray diffraction (XRD). Results reveal the presence of needle-like Sb inclusions preferentially aligned along the solidification direction within the InSb matrix. The onset and completion temperatures, as well as the melting enthalpy, were quantified for the composite. The observed anisotropy in the temperature-dependent electrical conductivity is ascribed to the short-circuiting effects induced by the oriented inclusions

Keywords: SEM, X-Ray Diffraction, eutectic composite, structure, thermal and electrical conductivity
PACS: 07.20.Fw, 61.05.cp, 68.37.Hk, 78.30.Fs, 81.30.-t

1. INTRODUCTION

Recent years have witnessed remarkable advances in high-performance thermoelectric (TE) materials. Although enhancing the figure of merit (ZT) and developing efficient TE devices for commercial applications remain challenging—requiring multidisciplinary efforts—the field holds significant promise [1–3]. Thermoelectric materials provide a sustainable route to convert waste heat into electricity, and achieving high ZT in a cost-effective manner is critical for practical energy generation. Mg_3Sb_2-based Zintl compounds are attractive candidates for high-performance TE materials due to their low-cost, non-toxic, and earth-abundant constituents. However, the low intrinsic ZT and degradation above 900 K limit the use of the pure phase. Investigating InSb+Mg_3Sb_2 eutectic composites, with a focus on the correlation between microstructure and TE properties, offers a pathway for optimizing performance [4–9]. Here, we report on the physico-chemical characteristics and TE potential of Mg_3Sb_2 Zintl compounds and InSb+Mg_3Sb_2 eutectic systems. In eutectic composites comprising InSb and 3d-transition metals, anisotropy in transport properties along the orientation of metallic needle-like inclusions is a defining characteristic. The parallel alignment of these metal needles with the crystallization direction leads to nonuniform semiconductor behavior, highlighting the importance of considering InSb–Sb composites. This study focuses on the synthesis and structural characterization of InSb–Sb eutectic composites. Diluted semiconductor materials based on A_3B_5 compounds combined with 3d-metal eutectic composites exhibit stable compositions and properties, making them promising candidates for spintronic applications. The anisotropic kinetic behavior observed in eutectic composites formed from InAs, InSb, GaSb, GaSe, and 3d-transition elements is predominantly governed by the orientation of metal inclusions.

Recently, unidirectionally solidified eutectic alloys have attracted interest for high-temperature applications. A critical requirement is the retention of the aligned microstructure during service. Extensive studies have investigated the high-temperature stability of such aligned composites [8–12]. Understanding the effect of thermal aging on eutectic alignment during coarsening is essential for ensuring reliable high-temperature performance.

2. EXPERIMENTAL RESULTS AND DISCUSSION

InSb-Mg_3Sb_2 eutectic composites were prepared by using the vertical Bridgman method. InSb and Mg_3Sb_2, form a lamellar eutectic. The eutectic concentration is 2.2 percent by weight Mg_3Sb_2. The rate of the crystallization front was about 1.2 mm/min. Metallographic examination revealed an eutectic structure with continuous rods of Sb in a matrix of lnSb, always oriented in the growth direction. This investigation focused on the undercooling behavior of antimony and indium antimonide phases, using materials like 99.8% and 99.999% Sb, primarily based on their purity. The InSb constituent was evaluated, and a semiconductor grade material with a nominal purity level of 99.999% was chosen. The eutectic of the InSb-Sb system is close to 69.5 mol% Sb. In order to construct the target, we first developed the eutectic composition—which is composed of Sb inclusions and an InSb single crystal matrix—using the Bridgman method. InSb-Sb eutectic specimens were made from ultrapure Sb (99.999%) and In (99.999%). In a quartz tube, the metals were vacuum-sealed in quantities that matched the InSb-Sb eutectic composition. The weight percentage of this composition [3] was 30.5 for InSb and 69.5 for Sb. After melting, the samples were moved from the hot zone to the lower temperature zone to solidify at different rates. The InSb-Sb eutectic was used to illustrate how interface demarcation can be applied to

131, H.Javid ave, AZ-1073, Baku
Institute of Physics
E-mail: jophphysics@gmail.com

the investigation of (directed) solidification of multiphase systems.

Raman analysis is an important tool to study atomic interactions in semiconductors and the dynamics of the crystal lattice [3]. The Raman spectra obtained in the InSb-Sb compositions only characterize the Sb-Sb bond (Fig.1)

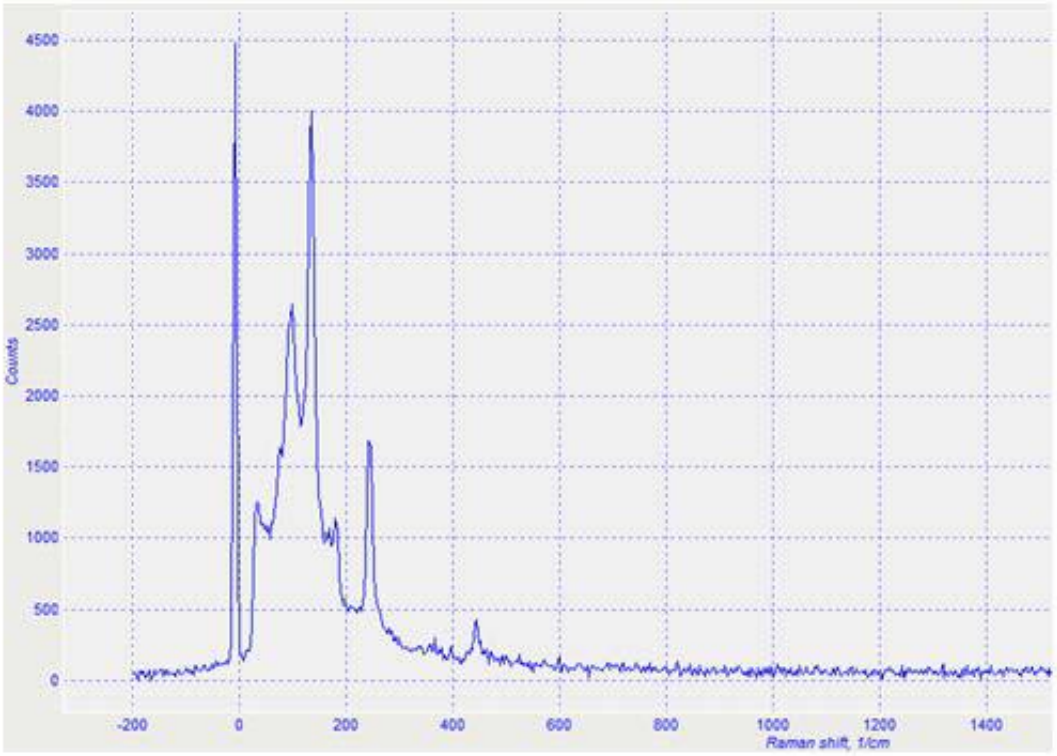

Fig. 1. Raman spectra of Sb-InSb eutectic composites

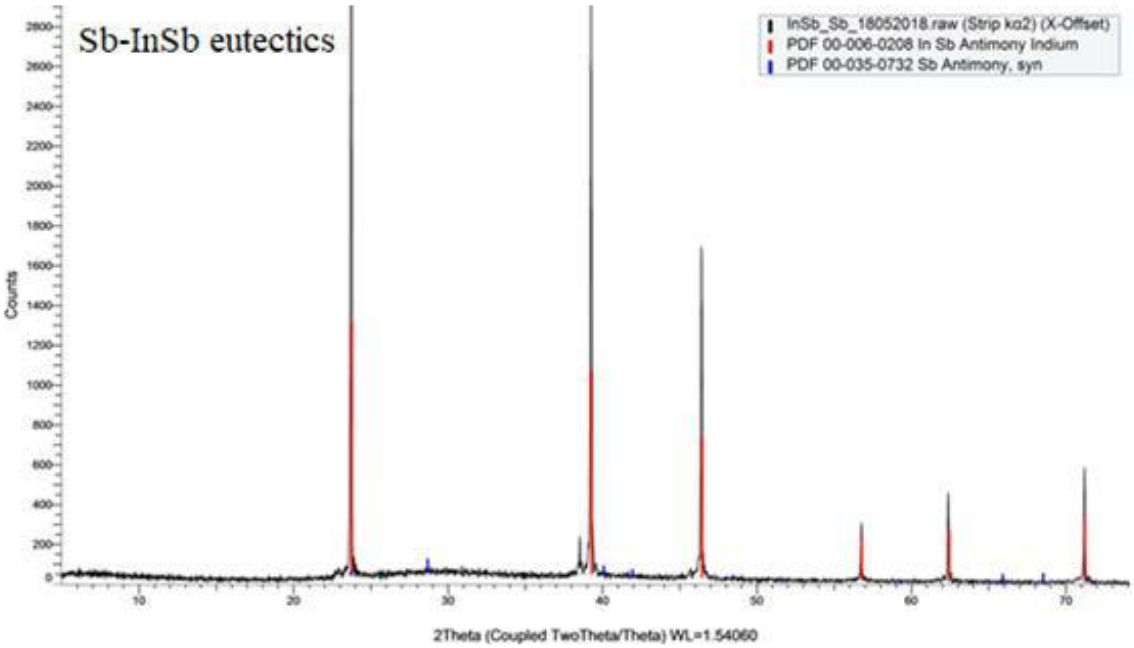

Fig. 2. X-ray spectrum of Sb-InSb eutectic composite.

Fig. 2 shows the diffraction patterns of the Sb-InSb eutectic composite. The X-ray phase analysis shows that the intense peaks corresponding to the (111), (220),(311), (400), (311), (422) and (511) Müller indices correspond to the matrix – InSb compound; the weak lines corresponding to the crystallographic parameters: a=4.121; c=5.467; c/a=1.327) compound and the 24; 29; 42; 49; 76 angles correspond to Sb [11]. The sharpness of the peaks in the diffractogram indicates the perfection of the composite.

Fig. 2 displays the diffraction patterns of the eutectic composite InSb-Sb. Data on the diffraction patterns for Sb and InSb compounds are also displayed in this picture. The length of the metal rods (1-1.8 μm in diameter) is 10-50μm in InSb-Sb. As it is seen from Fig. 2, the metal rods are evenly distributed in the matrix in the direction of crystallization. The metal rods are 10-150 μm in InSb-Sb and range in diameter from 1 to 1.8 μm. The metal rods are uniformly distributed throughout the matrix in the direction of crystallization, as seen in Fig. 3. Diffraction patterns ofthe InSb-Mg_3Sb_2 eutectic composite are shown in Fig. 3. The most intense peaks corresponding to the (111), (220), (311), (400), (311), (422) və (511) Muller index are identical to the InSb matrix, while the weak peaks found at $2\theta = 34.08^{o}$, 47.12^{o}, and 57^{o} coincide with the lamellar Mg_3Sb_2 line.

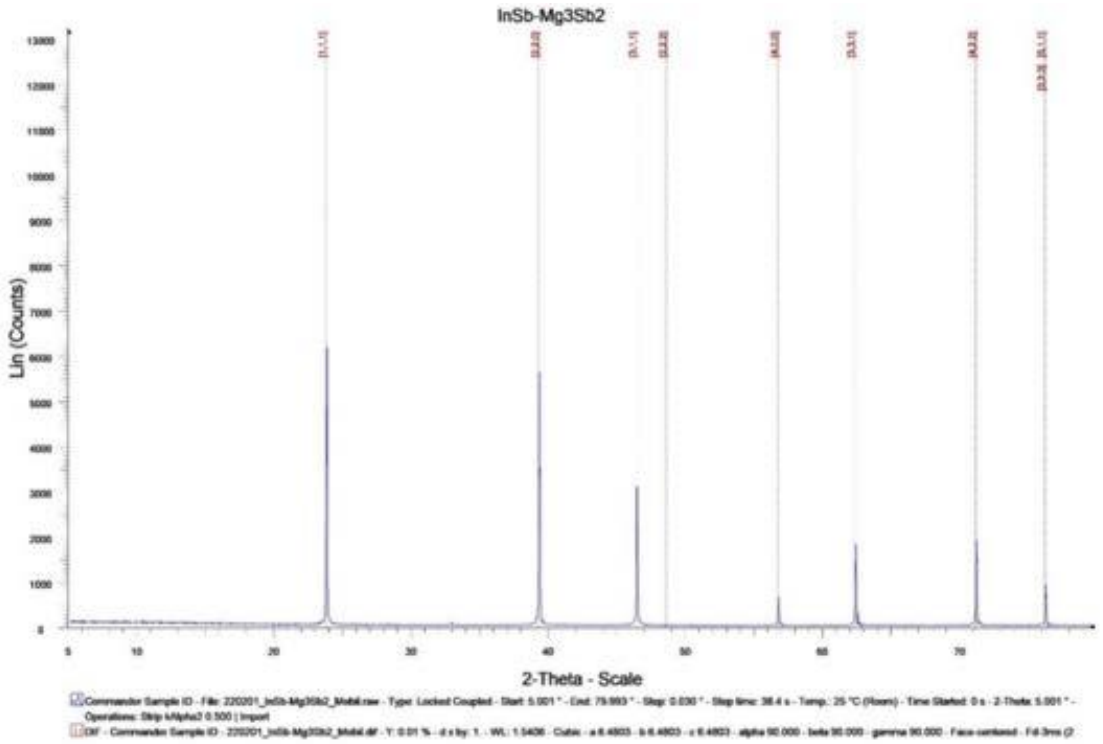

Fig. 3. X-ray spectrum of InSb+Mg_3Sb_2eutectic composite

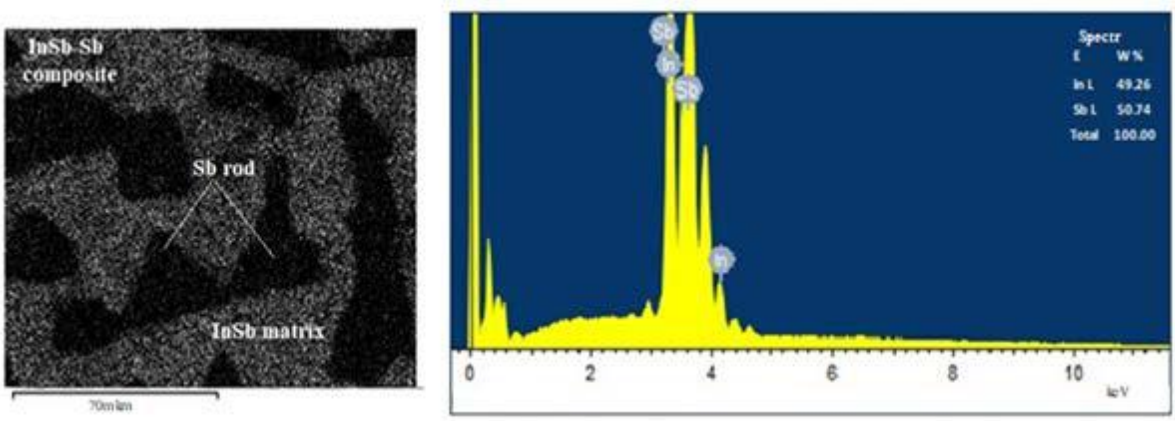

Fig. 4. X-ray spectra of Sb-InSb eutectic composite obtained with SEM–EDX from the rods and matrix phases along the lateral directions of the specimens.

The InSb-Sb eutectic's microstructure is highly sensitive to growth conditions during solidification. Directional solidification studies show rod morphology as stable growth form, but no extension to undercooled melt conditions has been done. The extent and shape of the coupled growth region remain unclear.The study evaluated undercooling and crystallization behavior of Sb and InSb, examining an eutectic mixture, exploring factors influencing undercooling, and characterizing solidification microstructures. The droplet emulsion technique increases undercooling potential for pure Sb, InSb, and an InSb-Sb alloy by dividing the bulk ingot into droplets of 10-150mkm, allowing for greater

undercooling. Higher cooling rates extend the metastable liquid state to lower temperatures, with droplet surface coating determining undercooling extent during solidification, a morphological transition from a rod to lamellar structure occurs due to a change in heat flow conditions. The thermal anisotropy of Sb encourages a change in growth orientation, causing the alignment of high conductivity planes and destroying the low energy orientation relationship between Sb rods and InSb matrix.

The microstructures of lnSb-Sb eutectic are illustrated by Fig. 4, which shows both longitudinal and transverse sections at various solidification rates. The size of rods was about 50 to 100 mkm in length and about 4 to 20 mkm in diameter, decreasing with increasing solidification rate. The rod-like Sb, when observed in transverse section, appeared triangular. The eutectic system lnSb-Sb was selected for the studies due to the phase diagram showing perfect eutectic behavior between lnSb and its constituent element Sb, with total miscibility of the components in the liquid state and very little solubility in the solid state. The starting ingredients are accessible in the high purities required for semiconductors, and the eutectic composition occurs at almost equal concentrations of InSb and Sb. When an InSb-Sb melt of eutectic compound is cooled below eutectic temperature, two phases crystallize simultaneously, forming an undercooled liquid layer rich in Sb around each crystallite. If excess Sb diffuses, a steady-state crystallization process can be maintained, allowing InSb crystallites and Sb crystallites to grow parallel until solidified.

The eutectic spacing, a measure of the fraction solidified within a droplet, indicates growth conditions during recalescence. It increases after nucleation until a transition zone, where droplet solidification is nonadiabatic due to nonzero undercooling.

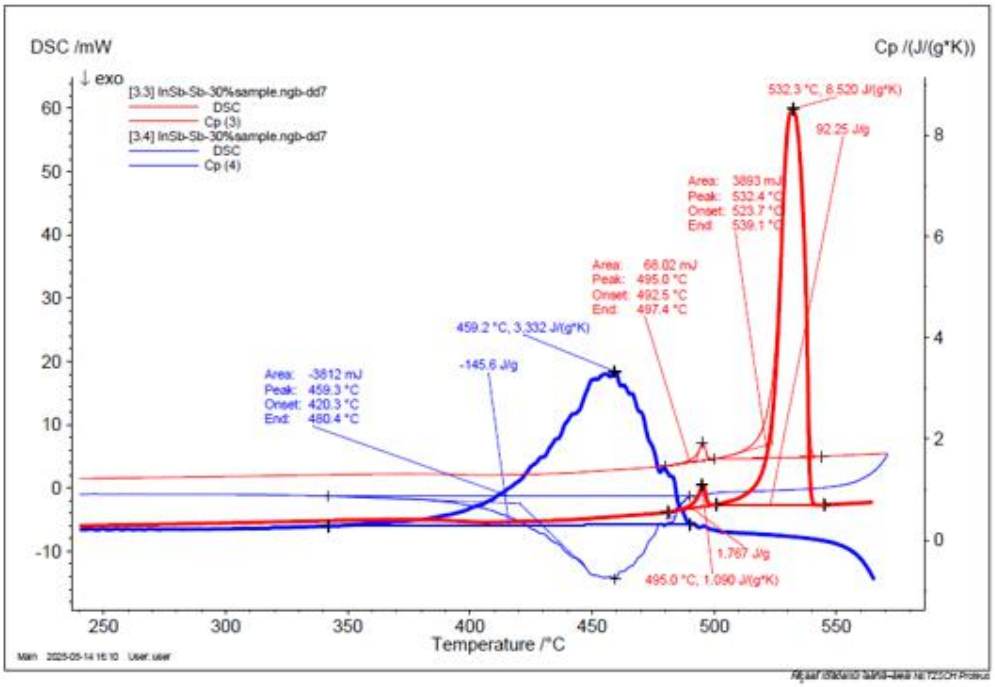

Fig.5. DSC curves for Sb-InSb eutectic composite.

The precise composition of an InSb ingot can facilitate the examination of the pure constituent, eliminating potential primary phase formation effects. Melt spinning or rapid heat extraction methods should be used with the eutectic alloy to assess the impact of exceeding the theoretical growth velocity limit for coupled growth.

The In-Sb binary system exhibits an eutectic reaction, forming a dual phase mixture of InSb and Sb, which serves as a crucial barrier for phonon transport.

The study successfully improved the thermoelectric performance of InSb-based alloys by optimizing eutectic content, achieving an unprecedented high ZT of 1.3 at 450^{0}C K.

Pik, K	DSC area, J/g	C_p, J/gK	
459.2^{0}C (p1)	92.25	8.520	endothermic
532.3^{0}C (p2)	68.02	1.09	endothermic

Differential scanning analysis (DSC) was used to monitor the sample's exothermic or endothermic behavior at high temperatures, revealing two endothermic peaks at 459.2^{0}C and 532.3^{0}C. InSb-Sb eutectic has a melting point of 532.3^{0}C K. The In-Sb phase diagram in Fig. 5 shows that peak p2 corresponds to InSb melting temperature, while peak p1 represents the melting point of the InSb-Sb eutectic. The microstructure observation confirms an InSb-Sb dual phase structure with Sb embedded in InSb matrix, but no typical lamellar eutectic structure was found.

Measurements have been made of the electrical and thermal conductivity (K) in relation to the alloys' two phases' structural arrangement (Fig.6). There has been a noticeable drop in the eutectic alloys' thermal conductivity. The interaction of phonons with the phase boundaries is most likely what causes the decrease in K [12]. The eutectic, with a lower melting point than its components, can reduce thermal conductivity and enhance ZT by introducing a suitable amount into the compound. Excess Sb was rationed to form an eutectic-included composite microstructure due to strong phonon scattering in the solid-liquid interface and enhanced ZT when melted to liquid.

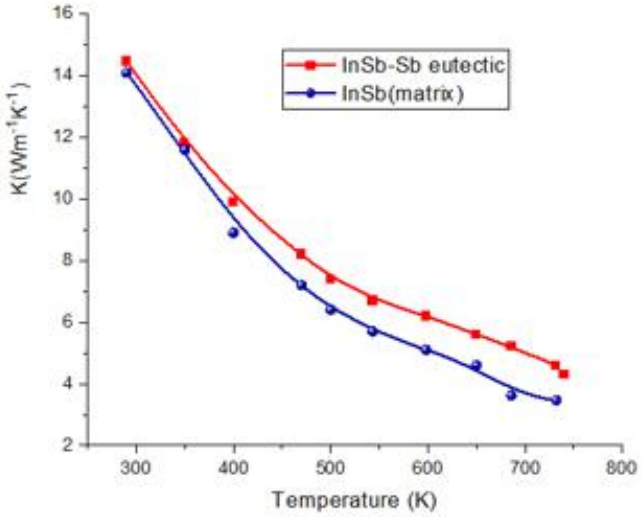

Fig.6. Thermal conductivity of InSb and Sb-InSb eutectic composite

Fig.7 display the findings of investigations into the temperature dependences of the electrical conductivity σ(T) determined at the various mutual directions of current (I), magnetic field (B), and crystallization direction.

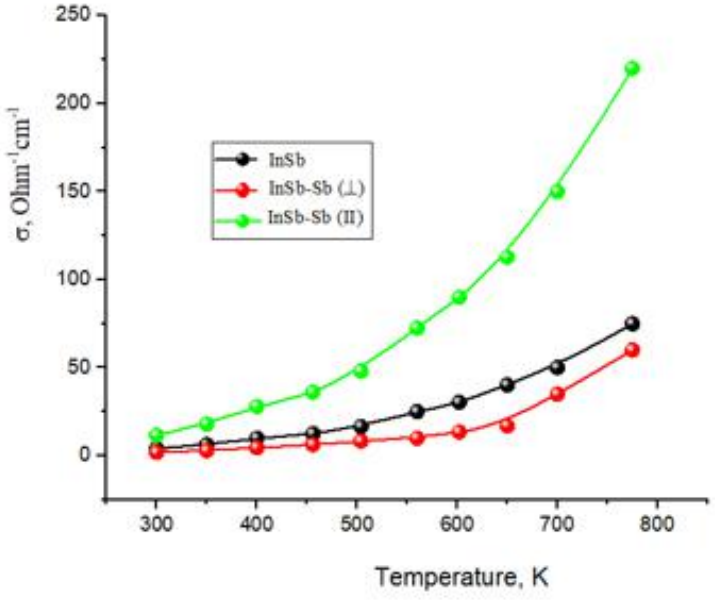

Fig. 7. Temperature dependence of electric conductivity for InSb and the Sb-InSb composite

The presence of regular metal crystalline inclusions in the semiconductor matrix causes anisotropy in the temperature dependence of the kinetic coefficients [13-17]. Electrical conductivity rises in the I || x direction due to shorting action by needle-shaped metallic inclusions, and it differs

greatly from σ(T) in the I⊥x direction. As the temperature rises, the coefficient of conductivity anisotropy falls, reaching σ||/σ⊥ = 3.

3. CONCLUSIONS

With no change in morphology from rod-like to lamellar, the study shows that rod size increases with solidification rate. X-ray analysis of lnSb-Sb, lnSb-Mg_3Sb_2 eutectic materials shows single crystalline development in both the Sb, Mg_3Sb_2 and lnSb matix, parallel to the hexagonal axis. Before evaluating the microstructure, metastable phases are found using X-ray diffraction techniques. By monitoring liquids' undercooling before to solidification, differential scanning analysis enables microstructural assessment.

[1] *M.V. Kazimov*. Synthesis and structural analysis of InSb-CrSb, InSb-Sb, GaSb-CrSb eutectic composites, Journal of Optoelectronic and Biomedical Materials Vol. 12, No.3,p.67-72, (2020), https://chalcogen.ro/67_KazimovMV.pdf

[2] *M.V. Kazimov, G.B. Ibragimov*. "Fabrication and performance characterization of Sb_2Se_3-GaSe eutectic systems". Semiconductor Physics, Quantum Electronics & Optoelectronics, 2024. V. 27, No 2. P. 184-188, http://journal-spqeo.org.ua/n2_2024/v27n2-p184-188.pdf

[3] *J.A. Graves*. Undercooling and Solidification Behavior in the InSb-Sb System, NASA CR-175013, September 1985, pp.216. https://ntrs.nasa.gov/citations/19860004885

[4] *M.V. Kazimov, G.B. İbragimov, G.I. İsakov*, at al.,Physical-chemical properties of InSb+Mg_3Sb_2 eutectic systems: Synthesis, Characterization, And Applications, Journal of Optoelectronic and Biomedical Materials,№14 (4), pp.187-190, (2022), https://chalcogen.ro/187_KazimovMV.pdf

[5] *M.V. Kazimov , D.H. Arasly*, et al., Magnetic and electrical properties of GaSb-CrSb eutectic system, Journal of Non-Oxide Glasses Vol. 12, No. 1, January - March 2020, p. 7 – 11, https://chalcogen.ro/7_KazimovMV.pdf

[6] *G.B. İbragimov*. Free-carrier absorption in quantum wires for boundary roughness scattering Journal of Physics Condensed Matter, 2003, 15(9), 1427–1435, http://journal-spqeo.org.ua/users/pdf/n3_2004/279-282_Ibragimov.pdf

[7] *M.R. Joya, P.S. Pizania, R.G. Jasinevicius*. Raman scattering investigation on structural and chemical disorder generated by laser ablation and mechanical microindentations of InSb single crystal, J. Appl. Phys. 100, (2006) 053518, https://doi.org/10.1063/1.2345052

[8] *M. Abaker, Nazar Elamin Ahmed, A. Saad, H.F. Khalil, E.M.M. Ibrahim, A.M. Adam.* Thermoelectric properties of Ga-doped InSb alloys, Vacuum, Volume 219, Part A, January2024,112761,https://www.sciencedirect.com/science/article/pii/S0042207X23009582?via%3Dihub

[9] *M.V. Kazimov*. X Ray Analysis Of InAs-CrAs Eutectic Systems, Arceng international Journal Of Architecture And Engineering, 3(1), 32-35, 2023, https://e-arceng.com/index.php/arceng/article/view/12

[10] *R.I. Alekberov, S.I. Mekhtiyeva, S.M. Mammadov, H.İ. Mammadova, B.G. Ibragimov, M.V. Kazımov, V.N. Poladova*. The influence of a hydrocarbon environment with aliphatic and cyclic chain structures on the volt-ampere characteristic of the Al-$Ge_{33}As_{17}S_{35}Se_{15}$-Te sandwich structure, Chalcogenide Letters, vol. 21, N 11 (2024), pp 927-931, https://doi.org/10.15251/CL.2024.2111.927

[11] *Q. Ye, R. Scheffler, J. Kumari, R. Leverenz.* Growth and characterization of single crystalline InSb nanowires for thermoelectric applications. NSTI Nanotech. 2007;1:237–240.

[12] *T. Berus, J. Goc, M. Nowak.* Preparation and electrical properties of InSb thin films heavily doped with tellurium, selenium and sulphur, Vol. 111, Issue 4, 1984, P. 351-366, https://doi.org/10.1016/0040-6090(84)90327-4

[13] *Okimura, Y. Koizumi , S. Kaida.* Electrical properties of p-type InSb thin films prepared by coevaporation with excess antimony, Vol.254, Issues 1–2, 1995, P. 169-174, https://doi.org/10.1016/0040-6090(94)06233-B

[14] *Xiaolin Cai, Jingsong Wei1*. Temperature dependence of the thermal properties of InSb materials used in data storage, Journal of Applied Physics 114, 083507 (2013) DOI: 10.1063/1.4819224

[15] *R.N. Rahimov, M.V. Kazimov, D.H. Arasly, A.A. Khalilova, I.Kh. Mammadov.* Features of Thermal and Electrical Properties of GaSb-CrSb eutectic composite , Journal Ovonic Research, 2017, v.13, No. 3, pp. 113-118.

[16] *M.M. Tagiyev, I.A. Abdullayeva, G.D. Abdinova, Kh.F. Aliyeva.* Thermoelectric Properties of an Extruded ZrO_2-Modified $Bi_{0.85}Sb_{0.15}$ Solid Solution. *Inorg Mater* **59**, 805–812 (2023). https://doi.org/10.1134/S0020168523080162

[17] *B.Ya. Balagurov, and G.A. Vinogradov*. Thermal conductivity of composites with needle-shaped inclusions, *Composites, Part A*, 2006, vol. 37, pp.1805–1814. https://doi.org/10.1016/j.compositesa.2005.08.01